

Grand Unification Scale CP Violating Phases And The Electric Dipole Moment

E. Accomando, R. Arnowitt and B. Dutta

*Center For Theoretical Physics, Department of Physics, Texas A&M University, College Station
TX 77843-4242*

(July, 1999)

Abstract

The question of CP violating phases in supersymmetry and electric dipole moments (EDMs) is considered within the framework of supergravity grand unification (GUT) models with a light ($\lesssim 1$ TeV) mass spectrum. In the minimal model, the nearness of the t-quark Landau pole automatically suppresses the t-quark cubic soft breaking phase at the electroweak scale. However, current EDM data require the quadratic soft breaking phase to be small at the electroweak scale unless $\tan\beta$ is small ($\tan\beta \lesssim 3$), and the EDM data combined with the requirement of electroweak symmetry breaking require this phase to be both large and highly fine tuned at the GUT scale unless $\tan\beta$ is small. Non minimal models are also examined, and generally show the same behavior.

I. INTRODUCTION

The Standard Model (SM) of strong and electroweak interactions possesses only one source of CP violating phases: the phase in the CKM matrix. While the physical origin of this phase remains unknown, it appears to satisfactorily account for the observed CP violation in the K meson system, and future data from B factories and high energy accelerators will be able to test its validity for B meson phenomena. It was early on realized that supersymmetric (SUSY) extensions of the Standard Model allowed for an array of new CP violating phases, and that these phases could give large contributions to the electric dipole moments [EDMs] of the electron and neutron [1], thus violating the known experimental bounds [2,3]. Several resolutions to this problem have been proposed, e.g. one might assume the phases are quite small i.e. $\lesssim O(10^{-2})$ [1,4], or suppress the diagrams by assuming the relevant SUSY particles are very heavy [5]. Both these suggestions a priori appear unsatisfactory, i.e. the first possibility would appear to require a significant amount of fine tuning, and the second would imply a SUSY spectrum in the TeV domain, possibly beyond the reach of even the LHC. More recently, it has been realized that some cancellations can occur in different contributions to the EDMs in certain parts of the SUSY parameter space

[6] which has led to considerable examination of this possibility [6–15]. In the minimal supersymmetric extension of the SM, the MSSM, (which we define as the low energy SUSY extension of the SM obtained by supersymmetrizing the particle spectrum with two Higgs doublets) this does appear to reduce the amount of fine tuning needed, allowing for larger phases. The existence of such phases could also have effects on other predictions of the MSSM [16–21], thus allowing future experimental checks of this idea.

In this paper we consider these questions from the viewpoint of supergravity (SUGRA) grand unified models (GUTs). In particular we consider gravity mediated models with R-parity invariance, where supersymmetry is broken in a hidden sector at some scale above the GUT scale M_G (presumably at the string or Planck scale M_{Pl}), the breaking being transmitted to the physical sector by gravity [22]. (For previous work from this viewpoint see Refs. [6,7,9,10,13,14].) Such models are much more constrained than the MSSM. Thus low energy properties are now determined by running the renormalization group equations (RGE) from M_G to the electroweak scale. CP violating phases that in the MSSM are arbitrary parameters now get correlated by the RGE, and no longer can be assigned independently to satisfy the EDM experimental bounds. Further, the radiative breaking of $SU(2) \times U(1)$ puts additional constraints on the CP violating phases. We find that as a consequence of these constraints, one must still fine tune some of the CP violating phases at the electroweak scale to be quite small, except for small regions of the parameter space with $\tan\beta$ close to its minimum value, or when SUSY masses are very large. Further, except for the lowest $\tan\beta$ a serious fine tuning develops at the GUT scale. These phenomena appear to be true both for the minimal mSUGRA model with universal soft breaking masses, and with nonuniversal soft breaking extensions. Hence the required smallness of the phases also tends to reduce the possibility of collateral evidence in other phenomena for their existence in SUGRA models.

In Sec.2, we discuss the solutions of the RGE for mSUGRA models and explain which phases that are large at the GUT scale get naturally suppressed at the electroweak scale (and which do not), and what the constraints of electroweak breaking imply both at the tree and 1-loop level. We then examine the amount of fine tuning needed to satisfy the existing EDM data, and what would be needed if those data were improved by a factor of 10 without finding any EDM. Sec.3 considers some effects of nonuniversal soft breaking on the EDM results.

In gravity mediated SUGRA models, the structure of the soft breaking parameters is to be deduced from the nature of the Kahler potential and gauge kinetic function at the GUT scale [22–24]. Thus what might be reasonable sizes for CP violating phases are presumably Planck scale physics questions. While at present there is no theory of such phenomena, one can still examine the general framework to see under what circumstances small or large phases might occur “naturally” at the GUT scale. This is analyzed in Sec.4, and a model with “naturally” small CP violating phases is discussed.

Concluding remarks are given in Sec.5.

II. EDM FOR MSUGRA MODELS

Supergravity GUT models with universal soft breaking of supersymmetry, mSUGRA, depend upon five parameters at the GUT scale: $m_{1/2}$ (the universal gaugino mass), A_0 (the cubic soft breaking mass, B_0 (the quadratic soft breaking mass), μ_0 (the Higgs mixing

parameter) and m_0 (the universal squark and slepton mass). Of these, the first four may be complex. However, it is always possible to make a phase transformation on the gaugino fields to make $m_{1/2}$ real, and since the reality is preserved by the RGE at 1-loop order, we will assume for now on that $m_{1/2}$ is real. We parameterize the remaining phases at M_G by :

$$A_0 = |A_0|e^{i\alpha_{0A}}; B_0 = |B_0|e^{i\theta_{0B}}; \mu_0 = |\mu_0|e^{i\theta_{0\mu}}. \quad (1)$$

The RGE allow one to determine the low energy parameters in terms of those of Eq.(1) and $m_{1/2}$ and m_0 . Thus at the electroweak scale, one obtains a different A parameter for each fermion (A_u, A_d, A_t, A_b, A_e and A_τ), real gaugino masses \tilde{m}_3, \tilde{m}_2 and \tilde{m}_1 for the $SU(3)_C, SU(2)_L$ and $U(1)_Y$ sectors, and complex B and μ parameters.

The EDM, d_f for fermion f, appears in the effective Lagrangian L_f as

$$L_f = -\frac{i}{2}d_f \bar{f} \sigma_{\mu\nu} \gamma^5 f F^{\mu\nu} \quad (2)$$

The basic diagrams giving rise to d_f are shown in Fig.1, and involve neutralino ($\tilde{\chi}_i^0, i=1,4$), chargino ($\tilde{\chi}_i^\pm, i=1,2$) and gluino (\tilde{g}) loops with squarks (\tilde{q}) and sleptons (\tilde{l}).

For the neutron dipole moment d_n one must also take into account the gluonic operators

$$L^G = -\frac{1}{3}d^G f_{abc} G_{a\mu\alpha} G_{b\nu}^\alpha \tilde{G}_c^{\mu\nu} \quad (3)$$

and

$$L^C = -\frac{i}{2}d^C \bar{q} \sigma_{\mu\nu} \gamma^5 T^a q G_a^{\mu\nu} \quad (4)$$

where $\tilde{G}_c^{\mu\nu} = \frac{1}{2}\epsilon^{\mu\nu\alpha\beta} G_{c\alpha\beta}$, f_{abc} are the SU(3) structure constants and $T^a = \frac{1}{2}\lambda^a$, where λ^a are the SU(3) Gell-Mann matrices. In addition to the diagrams of Fig.1 with γ replaced by g , operators of Eqs.(2-4) receive contributions from the two loop Barr-Zee diagrams of Fig.2 [25], and the two loop Weinberg type diagram of Fig.3 [26]. For the neutron dipole moment one must use the QCD factors $\eta^{ED}, \eta^G, \eta^C$ to evolve the results at the electroweak scale down to 1 GeV [27].

The calculation of d_n suffers from QCD uncertainties from several sources. These include: (1) How to relate the quark moments d_u, d_d to the neutron moment d_n . We use here the non relativistic quark model relation. (For other approaches see Ref. [14].)

$$d_n = \frac{1}{3}(4d_d - d_u) \quad (5)$$

(2) How to relate color and gluonic contributions to the electric dipole moment. We use here the ‘‘naive dimensional analysis’’ of Ref. [28].

(3) Uncertainty in m_s , the strange quark mass, which affects the determination of m_u and m_d . While the quark mass ratios are well known [29],

$$\frac{m_u}{m_d} = 0.553 \pm 0.043; \quad \frac{m_s}{m_d} = 18.9 \pm 0.8 \quad (6)$$

one has $m_s = (175 \pm 25)\text{MeV}$ from QCD sum rules and $m_s = (100 \pm 20 \pm 10)\text{ MeV}$ (2 GeV) from the quenched lattice calculation [30] (Using unquenched approximation one expects an even smaller value [31]).

Thus the values of d_n calculated below have a significant uncertainty. In spite of this, it is useful to see the effect on the SUSY parameter space of simultaneously imposing the experimental constraints on both d_n and d_e and we will discuss below how the uncertainty in m_s effects these constraints.

To specify our phase conventions, we give the mass matrices for the particles entering in Fig.1. With a convenient choice of phases, the chargino and the neutralino mass matrices are:

$$M_{\chi^\pm} = \begin{pmatrix} \tilde{m}_2 & \sqrt{2}M_W \sin\beta \\ \sqrt{2}M_W \cos\beta & -|\mu|e^{i\theta} \end{pmatrix} \quad (7)$$

$$M_{\chi^0} = \begin{pmatrix} \tilde{m}_1 & 0 & a & b \\ 0 & \tilde{m}_2 & c & d \\ a & c & 0 & |\mu|e^{i\theta} \\ b & d & |\mu|e^{i\theta} & 0 \end{pmatrix} \quad (8)$$

where $a = -M_Z \sin\theta_W \cos\beta$, $b = M_Z \sin\theta_W \sin\beta$, $c = -\cot\theta_W a$, $d = -\cot\theta_W b$, $\tan\beta = v_2/v_1$ ($v_{1,2} = |\langle H_{1,2} \rangle|$) and θ_W is the weak mixing angle. The phase θ is given by

$$\theta = \epsilon_1 + \epsilon_2 + \theta_\mu \quad (9)$$

where at the electroweak scale, $\langle H_{1,2} \rangle = v_{1,2} e^{i\epsilon_{1,2}}$, and $\mu = |\mu|e^{i\theta_\mu}$. The squark mass matrices may be written as

$$M_{\tilde{q}}^2 = \begin{pmatrix} m_{qL}^2 & e^{-i\alpha_q} m_q (|A_q| + |\mu|R_q e^{i(\theta+\alpha_q)}) \\ e^{i\alpha_q} m_q (|A_q| + |\mu|R_q e^{-i(\theta+\alpha_q)}) & m_{qR}^2 \end{pmatrix} \quad (10)$$

where m_q , e_q are the quark mass and charge,

$$m_{qL}^2 = m_Q^2 + m_q^2 + (1/2 - e_q \sin^2\theta_W) M_Z^2 \cos 2\beta \quad (11)$$

$$m_{qR}^2 = m_U^2 + m_q^2 + e_q \sin^2\theta_W M_Z^2 \cos 2\beta \quad (12)$$

$A_q = |A_q|e^{i\alpha_q}$, m_Q^2 and m_U^2 are given in Ibanez et al. [32] and $R_q = \cot\beta(\tan\beta)$ for u(d) quarks. Similar expressions hold for slepton masses, with phases α_l . Our sign conventions for A_q and μ are those of Ref. [35].

The condition for electroweak symmetry breaking is obtained by minimizing the effective potential V_{eff} with respect to v_1 , ϵ_1 , v_2 and ϵ_2 . The Higgs sector of V_{eff} is

$$V_{eff} = m_1^2 v_1^2 + m_2^2 v_2^2 + 2|B\mu| \cos(\theta + \theta_B) v_1 v_2 + \frac{g_2^2}{8} (v_1^2 + v_2^2)^2 + \frac{g_1^2}{8} (v_2^2 - v_1^2)^2 + V_1 \quad (13)$$

where V_1 is the one loop contribution, $m_i^2 = \mu^2 + m_{H_i}^2$ and $m_{H_{1,2}}^2$ are the $H_{1,2}$ running masses. For particles of spin j one has

$$V_1 = \frac{1}{64\pi^2} \sum_a C_a (-1)^{2j_a} (2j_a + 1) m_a^4 \left(\ln \frac{m_a^2}{Q^2} - \frac{3}{2} \right) \quad (14)$$

where C_a is the color degree of freedom of the a^{th} particle. In the following we choose the low energy scale Q to be m_t (175 GeV), and include the full third generation states, t , b and τ in V_1 . This allows an examination of the large $\tan\beta$ domain.

We view the minimization equations of V_{eff} as equations to determine the Higgs VEVs i.e. $v_1, v_2, \epsilon_1, \epsilon_2$. Thus in the tree approximation, the extrema equations $\partial V_{eff}/\partial \epsilon_i = 0$ yield $2|B\mu|\sin(\theta + \theta_B) = 0$, and hence the minimum of V_{eff} requires

$$\theta = \pi - \theta_B \quad (15)$$

(the choice of $\theta = -\theta_B$ leads to a maximum). The one loop corrections depend only on the mass eigenvalues, and hence from Eq.(10) only on the phase $\theta + \alpha_q$ and $\theta + \alpha_l$. Thus, at the one loop level, one gets a correction to Eq.(15) of the form [16,17]

$$\theta = \pi - \theta_B + f_1(\pi - \theta_B + \alpha_q, \pi - \theta_B + \alpha_l) \quad (16)$$

where f_1 is the one loop correction with θ approximated by its tree value, Eq.(15). As we will see, this correction can become significant for large $\tan\beta$. The EDMs however depend on both the mass eigenvalues and the rotation matrices. Hence they will depend on $\theta + \alpha_q$ and α_q separately, with θ determined by the electroweak symmetry breaking condition in Eq.(16).

The current experimental 90% C.L. upper bounds on d_n [3] and d_e [2] are

$$(d_n)_{exp} < 6.3 \times 10^{-26} ecm; \quad (d_e)_{exp} < 4.3 \times 10^{-27} ecm \quad (17)$$

In discussing the data, it is convenient to define the quantity

$$K = \log_{10} \left| \frac{d_f}{(d_f)_{exp}} \right| \quad (18)$$

Thus $K = 0$ corresponds to a theoretical value which saturates the current experimental bound, while $K = -1$ would represent the case, should the experimental bounds be reduced by a factor of 10. As pointed out in Refs. [6–15], various cancellations can occur among the different contributions to the EDM. This is illustrated in Fig.4 where K is plotted vs. m_0 for the electron dipole moment (eEDM). We note that eventually for very large m_0 , the curves fall below the $K = 0$ bound (as expected). Further the allowed range of m_0 (so that $K \leq 0$) decreases with increasing $\tan\beta$ (and the allowed range would become very small should $K = -1$, i.e. the experimental bounds be reduced by a factor of 10). In addition, the position of the dips moves to lower m_0 with increasing $\tan\beta$. This happens due to the fact that the regions on the right of the dips are dominated by the contribution from the chargino diagram. As $\tan\beta$ increases, the contribution from the chargino diagram increases much more than the contribution from the neutralino diagram. However, a decrease in m_0 increases the neutralino diagram much more than the chargino diagram. As a result the dips shift towards the smaller m_0 value for larger $\tan\beta$. We use negative values (arising from the factor π in the Eq. 15) of μ to satisfy the experimental constraints on the BR of $b \rightarrow s\gamma$ [33,34].

We begin our analysis by examining the RGE to determine what GUT scale parameters lead to acceptable CP violating phases at the electroweak scale. We have used Ref. [35] for the RGE relating the GUT scale parameters to the parameters at the electroweak scale. In general, the RGE must be solved numerically and all results given below are obtained by accurate numerical integration. However, approximate analytic solutions can be found for

low and intermediate $\tan\beta$ (neglecting b and τ Yukawa couplings) or for the $SO(10)$ limit of very large $\tan\beta$ (neglecting the τ Yukawa coupling). These analytic solutions give some insight into the nature of the more general numerical results.

The solution for the $A_t(t)$ parameter in the low and intermediate $\tan\beta$ case can be cast in the form [36]

$$A_0 = \frac{A_R(t)}{D_0} + \frac{H_3(t)}{F(t)}m_{1/2} \quad (19)$$

where A_R is the residue at the t-quark Landau pole,

$$A_R = A_t + m_{1/2}(H_2(t) - \frac{H_3(t)}{F(t)}) \quad (20)$$

and

$$D_0 = 1 - 6\frac{F(t)}{E(t)}Y(t). \quad (21)$$

Here $t = 2\ln(M_G/Q)$, the form factors E , F , H_2 and H_3 are real and are defined in [32] and $Y(t) = h_t/16\pi^2$, where h_t is the t-quark Yukawa coupling constant. D_0 vanishes at the t-quark Landau pole (for $Q=m_t$, $D_0 \cong 1 - (m_t/200\sin\beta)^2$) and is generally small (i.e. $D_0 \lesssim 0.2$ for $m_t = 175$ GeV). The imaginary part of Eq.(19) gives:

$$D_0|A_0|\sin\alpha_{0A} = |A_t|\sin\alpha_t. \quad (22)$$

Thus even if $\alpha_{0A} = \pi/2$, α_t at the electroweak scale will be generally suppressed due to the smallness of D_0 , i.e. the RGE naturally make the phase α_t small due to the nearness of the Landau pole. (This result has been previously observed, for low $\tan\beta$ in [9].) The approximate $SO(10)$ solution with large $\tan\beta$ (where $Y_t \cong Y_b$) gives a similar analytic form for $A_t(t) \cong A_b(t)$ with the factor 6 replaced by 7 in Eq.(21). Thus the suppression effect on α_t occurs over the entire $\tan\beta$ domain. These effects thus allow α_{0A} to be large without a priori violating the experimental EDM bounds.

In contrast there is no analogous RGE suppression effect in the first generation A parameters A_u , A_d and A_e . From the RGE, one finds that A_u has the form of Eq.(19) for low and intermediate $\tan\beta$ with the factor 6 replaced by 1 in Eq.(21). Now $D_0 \simeq 1$ and no suppression effect occurs for α_u at the electroweak scale in the analogue of Eq.(22). However, the EDMs are not very sensitive to the first generation α_u , α_d , α_e and one can have large values of these parameters without violating the experimental bounds in a reasonable region of the SUSY parameter space.

From the RGE, one sees that the phase of the μ parameter does not run at the 1-loop level, i.e. $\theta_{0\mu} = \theta_\mu$, where θ_μ is the phase at the electroweak scale. Thus a large GUT scale phase will lead to a large electroweak scale phase. However, as seen in Eqs.(7-10), θ_μ enters only in the combination θ , and θ is determined in terms of θ_B , α_l and α_q by the minimization of the effective potential, as given in Eq.(16). Thus (with our choice of the phases in the mass matrices) θ_μ does not enter in the EDMs.

The EDMs, however are highly sensitive to θ_B , which by Eq.(16), enters into all the diagrams, and over most of the parameter space, θ_B must be small to satisfy the EDM

experimental bounds. This is illustrated in Fig.5 where we have plotted the eEDM K vs. θ_B . We see that θ_B can be large i.e. $\theta_B \simeq 0.08$, for low $\tan\beta = 3$, though it becomes smaller for higher $\tan\beta$. However, even for $\tan\beta = 3$, the range $\Delta\theta_B$ of θ_B so that $K \leq 0$ is very small i.e. $\Delta\theta_B \lesssim 0.02$ (and θ_B would become quite fine tuned if the experimental bound were reduced by a factor of 3 i.e. $K = -0.5$). Figs.6 show that $\Delta\theta_B$ remains small for $m_{1/2} \lesssim 350$ GeV ($m_{\tilde{g}} \lesssim 1$ TeV) and only relaxes somewhat when $m_{1/2} \simeq 700$ GeV ($m_{\tilde{g}} \lesssim 2$ TeV). In this figure we have plotted the $K \leq 0$ regions as a function of θ_B and $m_{1/2}$ for three different values of $\tan\beta$. Since the contribution from the chargino diagram increases with $\tan\beta$, the larger $\tan\beta$ requires a smaller phase to produce the necessary cancellation between the chargino and the neutralino diagrams.

The RGE allow us to examine the significance of the above results at the GUT scale. The RGE for B and A_t can be solved in the low and intermediate $\tan\beta$ regime to obtain

$$B = B_0 - \frac{1}{2}(1 - D_0)A_0 - \Phi m_{1/2} \quad (23)$$

where

$$\Phi = -\frac{1}{2}(1 - D_0)\frac{H_3}{F} + [3h_2 + \frac{3}{5}h_1]\frac{\alpha_G}{4\pi} \quad (24)$$

$h_i = t/(1 + \beta_i t)$, $\alpha_G \cong 1/24$ is the GUT gauge coupling constant and β_i are the MSSM beta functions. The real and the imaginary parts of Eq.(23) give:

$$|B|\sin\theta_B = |B_0|\sin\theta_{0B} - \frac{1}{2}(1 - D_0)|A_0|\sin\alpha_{0A} \quad (25)$$

$$|B|\cos\theta_B = |B_0|\cos\theta_{0B} - \frac{1}{2}(1 - D_0)|A_0|\cos\alpha_{0A} - \Phi m_{1/2} \quad (26)$$

Eqs.(25,26) can be viewed as determining the electroweak scale values of $|B|$ and θ_B in terms of the GUT input parameters. Thus θ_B depends upon both the initial phase θ_{0B} and the A_0 phase α_{0A} . Alternatively, one may use Eqs.(25,26) to impose electroweak scale phenomenological constraints on the allowed GUT parameters. The requirement that the GUT theory gives rise to electroweak symmetry breaking gives

$$|B| = \frac{1}{2}\sin 2\beta \frac{m_3^2}{|\mu|} \quad (27)$$

where $m_3^2 = \mu_1^2 + \mu_2^2$ and $\mu_i^2 = |\mu|^2 + m_{H_i}^2 + \Sigma_i$. (Here $m_{H_i}^2$ are the running Higgs masses at the electroweak scale, $|\mu|$ is determined by electroweak breaking and Σ_i are the one loop corrections [37].) In addition, we have seen that the experimental bounds on the EDMs restrict θ_B to be small, i.e. $|\theta_B| \lesssim 0.1$ (and usually much smaller) and the allowed range, $\Delta\theta_B$, that satisfies the EDMs is quite small. These conditions put severe constraints on the GUT scale theory which we now discuss.

Consider first the case where $\tan\beta$ is very close to its minimum value e.g. $\tan\beta=2$. Here $1/2\sin 2\beta$ is not small and by Eq.(27), $|B|$ is of normal size. Eq.(25) then implies that θ_B and θ_{0B} are of roughly the same size (even for $\alpha_{0A} = \pi/2$) as previously noted

in Ref. [9]. Thus a reasonable GUT theory requires one only to justify the size of θ_{0B} . However, as $\tan\beta$ increases, $1/2\sin 2\beta$ decreases, and unless μ becomes anomalously small or m_3^2 anomalously large, Eq.(27) implies that $|B|$ becomes small. Thus the lefthand side of Eq.(25) becomes small (and to first approximation can be neglected), and Eq.(25) implies that θ_{0B} is determined by α_{0A} mainly, i.e. θ_{0B} is large if α_{0A} is large. This result is illustrated in Fig.7 where θ_{0B} is plotted vs. θ_B . We see that since θ_B is small for all $\tan\beta$, θ_{0B} is in general large, e.g. even for $\tan\beta = 3$ one has $\theta_{0B} \simeq 0.8$.

Returning to Eq.(25), we see, however, that $\Delta\theta_{0B}$, the range of values of θ_{0B} that will satisfy the EDM constraints, is very small. Thus for fixed A_0 , Eq.(25) implies for large $\tan\beta$ that

$$\Delta\theta_{0B} \simeq \frac{|B|}{|B_0|} \Delta\theta_B \ll \Delta\theta_B \quad (28)$$

and since $\Delta\theta_B$ is small, $\Delta\theta_{0B}$ will be very small. This is illustrated in Fig.8 where the allowed values of θ_{0B} for $K \leq 0$ are plotted vs. $m_{1/2}$ for d_e and d_n for $\tan\beta=3, 10, 20$. We see that the phenomenological constraints at the electroweak scale imply that θ_{0B} is both large and its value is sharply fine tuned (unless α_{0A} is small, SUSY masses are large or $\tan\beta$ is small). One may alternatively view this from the ‘‘top down’’: if Planck physics determines α_{0A} and θ_{0B} to be large and fixed, then if the model is to achieve electroweak symmetry breaking with EDMs below existing bounds, there will be a fine tuning of other GUT scale parameters (unless $\tan\beta$ is small or the SUSY masses are large).

As discussed above, there are a number of uncertainties in the calculation of the neutron EDM. Fig.9 illustrates the effects of varying the d-quark mass in a plot of the region allowed by the experimental EDM bounds ($K \leq 0$) in the $m_0 - m_{1/2}$ plane for $\theta_B = 0$, $|A_0| = 300$ GeV, $\alpha_{0A} = \pi/2$, $\tan\beta=3$. The bound on d_e already excludes all regions below the lower solid curve, while the d_n bound excludes regions to the left of the upward running curves for $m_d = 5$ MeV (dotted), $m_d = 8$ MeV (solid), $m_d = 12$ MeV (dashed). Thus the combined exclusion region increases from $m_{1/2} \gtrsim 260$ GeV to $m_{1/2} \gtrsim 440$ GeV as m_d increases, a significant change. In the other figures in this paper we have used the middle value of $m_d = 8$ MeV corresponding to $m_s \simeq 150$ MeV.

In Fig.9, we have chosen $\theta_B = 0$. As one increases θ_B , one will eventually arrive at a neutralino-chargino cancellation region, and this will reduce the values of m_0 and $m_{1/2}$ which are excluded. Further, for low $\tan\beta$ this cancellation can occur at relatively large θ_B (i.e. $\theta_B \simeq 0.2$) as shown in Ref. [9]. Alternatively, increasing $\tan\beta$ can also cause this cancellation, as the loop corrections, Eq.(16), become large with large $\tan\beta$ and the contribution from the chargino diagram increases with $\tan\beta$. This is illustrated for $\tan\beta=20$ in Fig.10 where the d_n curve for $K = 0$ (solid) bends downward below $m_0=500$ GeV when $200 \text{ GeV} < m_{1/2} < 400$ GeV, showing in this exceptional type situation that one can satisfy the EDM constraints with a light particle spectrum and large $\tan\beta$. Note that the cancellation can occur for a relatively wide band of $m_{1/2}$, and persists even for $K = -0.5$.

The regions of the SUSY parameter space that get eliminated by a joint imposition of the experimental bounds on the d_e and d_n are sensitive, of course, to the choice of the parameters. Thus in Figs.6 one sees that for $m_0 = 100$ GeV, one requires $m_{1/2} \gtrsim 350$ GeV ($m_{\tilde{g}} \gtrsim 1\text{TeV}$) to jointly satisfy the d_e and d_n bounds, and this requirement is roughly independent on $\tan\beta$. Fig.11 shows that if m_0 is increased to 250 GeV one requires now

$m_{1/2} \gtrsim 160$ GeV ($m_{\tilde{g}} \gtrsim 450$ GeV) to satisfy both bounds, i.e. if m_0 is increased, the lower bound on $m_{1/2}$ is decreased as expected. However, if $|A_0|$ is increased, it is not necessary that the allowed domain of $m_{1/2}$ increases. This is illustrated in Fig.12 for the choice $|A_0|=800$ GeV, $m_0=100$ GeV. The increase of $|A_0|$ raises the allowed values of θ_B for both d_e and d_n , but the raising of d_e is larger causing the joint allowed domain to require $m_{1/2} \gtrsim 550$ GeV ($m_{\tilde{g}} \gtrsim 1.5$ TeV).

In order to exhibit the size of $|\mu|$, we have plotted $|\mu|$ as a function of $m_{1/2}$ for $m_0=100, 300$ and 700 GeV in Fig.13. The EDM constraints have not been imposed in Fig.13, but from Fig.6a, one sees that they are satisfied at least for $m_0=100$ GeV for d_e for essentially the entire $m_{1/2}$ range (which allows $\theta_B \simeq 0.08$). Note that $|\mu|$ is large (i.e. $|\mu|^2/M_Z^2 \gg 1$) over the full $m_{1/2}$ domain so that one is generally in the gaugino scaling domain.

III. NONUNIVERSAL SOFT BREAKING

There are three types of nonuniversalities that might be considered in SUGRA models: nonuniversal gaugino masses at M_G , nonuniversal scalar masses at M_G and generation off diagonal cubic soft breaking matrices A_{ij} and scalar mass matrices m_{ij}^2 . We will discuss here briefly the first two possibilities, a more detailed analysis will be given in a later paper [38]. (The third type of non universality has the possibility of generating ϵ and ϵ'/ϵ CP violations independent of the CKM phase [39].)

In general, the U(1), SU(2) and SU(3) gaugino masses at M_G can have the form

$$m_{1/2i} = |m_{1/2i}|e^{i\phi_i}; i = 1, 2, 3 \quad (29)$$

A convenient phase choice is to set the SU(2) phase to zero: $\phi_2 = 0$, and hence the chargino mass matrix, Eq.(7), is unchanged. The remaining phases produce effects in the RGE for $A_t(t)$:

$$A_t = D_0 A_0 + \sum_i \Phi_{ti} |m_{1/2i}| e^{i\phi_i} \quad (30)$$

and hence the imaginary part gives

$$|A_t| \sin \alpha_t = |A_0| D_0 \sin \alpha_{0A} + \sum_i \Phi_{ti} |m_{1/2i}| \sin \phi_i \quad (31)$$

Thus the Landau pole factor D_0 still suppresses any large phase α_{0A} at the GUT scale, though α_t may become large due to the ϕ_i phase which does not run at one loop order and hence is not suppressed. This phenomena can affect d_n .

A second effect occurs in the neutralino mass matrix which now reads

$$M_{\chi^0} = \begin{pmatrix} |\tilde{m}_1| e^{i\phi_1} & 0 & a & b \\ 0 & \tilde{m}_2 & c & d \\ a & c & 0 & |\mu| e^{i\theta} \\ b & d & |\mu| e^{i\theta} & 0 \end{pmatrix} \quad (32)$$

where $\theta = \epsilon_1 + \epsilon_2 + \theta_\mu$. Thus ϕ_1 effects any neutralino-chargino cancellations in d_e and d_n . An example is illustrated in Fig.14. One sees that θ_B can be large but is still tightly

constrained to satisfy the experimental EDM bound (i.e. $\Delta\theta_B \simeq 0.02$). One is again led to a fine tuning at the GUT scale.

As an example of nonuniversal sfermion masses, we consider an SU(5)-type model where the GUT group possesses an SU(5) subgroup with matter embedded in the usual way in $10 + \bar{5}$ representations. We also assume the first two generations remain universal to suppress flavor changing neutral currents. The Higgs masses have the form at M_G

$$m_{H_1}^2 = m_0^2(1 + \delta_1); \quad m_{H_2}^2 = m_0^2(1 + \delta_2) \quad (33)$$

while the third generation 10 representation (containing $\tilde{t}_L, \tilde{t}_R, \tilde{b}_L, \tilde{\tau}_R$) and the $\bar{5}$ (containing $\tilde{b}_R, \tilde{\nu}_\tau, \tilde{\tau}_L$) masses are parametrized by

$$m_{10}^2 = m_0^2(1 + \delta_{10}); \quad m_{\bar{5}}^2 = m_0^2(1 + \delta_5) \quad (34)$$

Here the $\delta_i \geq -1$ represent the deviations from the universality. In addition the third generation cubic soft breaking parameters are A_{0t} and $A_{0b} = A_{0\tau}$.

One may use the non universal sfermion and Higgs masses to soften the effects of the experimental EDMs. This is illustrated in Fig.15 where the $K=0$ constraint is imposed in the $m_0 - m_{1/2}$ plane for a choice of δ_i parameters. For $\delta_i = 0$, the d_n curve would continue to rise for small $m_{1/2}$ as seen in Fig.9, rather than turn over as in Fig.15. For example, for $m_{1/2}=220$ GeV and $\tan\beta=5$, $K(d_n) < 0$ occurs for $m_0 > 580$ GeV in the non universal case, whereas $K(d_n) < 0$ occurs for $m_0 > 750$ GeV in the universal case. The particular set of δ_i s in the Fig.15 is chosen to reduce the stop and the sbottom mass and to satisfy the requirement of the radiative electroweak symmetry breaking. The lower stop and sbottom mass increases the Weinberg type diagram which has a subtractive effect in the net nEDM magnitude.

IV. SUGRA MODEL OF SMALL PHASES

While choosing the CP violating phases to be small, i.e. $\phi_i \simeq 10^{-2}$, to satisfy the EDM constraints appears to be artificial in the low energy MSSM, it is possible that a natural model of this type can arise in SUGRA GUT models.

SUGRA models depend on three functions of the chiral fields Φ_α : $f_{\alpha\beta}(\Phi_\alpha)$ the gauge kinetic energy, $K(\Phi_\alpha, \Phi_\alpha^\dagger)$ the Kahler potential and $W(\Phi_\alpha)$ the superpotential. One assumes a hidden sector exists where some fields, e.g. moduli or dilaton, Φ_i grow VEVs of Planck size to break supersymmetry i.e.

$$x_i = \kappa \langle \Phi_i \rangle = O(1) \quad (35)$$

where $\kappa^{-1} = M_{Pl} = 2.4 \cdot 10^{18}$ GeV. Thus one can write $\{\Phi_\alpha\} = \{\Phi_i, \Phi_a\}$ where Φ_a are the physical sector fields. One might expand the Kahler potential in a power series of the physical fields:

$$K = \kappa^{-2} c^{(0)} + (c_{ab}^{(2)} \Phi_a \Phi_b + \frac{1}{M} c_{abc}^{(3)} \Phi_a \Phi_b \Phi_c + \dots) + (\tilde{c}_{ab}^{(2)} \Phi_a \Phi_b^\dagger + \frac{1}{M} \tilde{c}_{abc}^{(3)} \Phi_a^\dagger \Phi_b \Phi_c + \dots) \quad (36)$$

where M is a large mass. The $c^{(i)}, \tilde{c}^{(i)}$ are dimensionless and we assume them to be $O(1)$. The first parenthesis is holomorphic, and can be transferred to the superpotential by a Kahler transformation giving rise to the μ term:

$$W \rightarrow W + \kappa^2 W (c_{ab}^{(2)} \Phi_a \Phi_b + \frac{1}{M} c_{abc}^{(3)} \Phi_a \Phi_b \Phi_c + \dots) \quad (37)$$

The leading additional terms on the right occur when W there is replaced by its VEV ($\kappa^2 \langle W \rangle \simeq m_{3/2}$) and one of the fields in the cubic term, e.g. Φ_c , has a GUT scale VEV. Then $W \rightarrow W + \mu_{ab} \Phi_a \Phi_b$, where

$$\mu_{ab} = (c_{ab}^{(2)} + \frac{M_G}{M} c_{abc}^{(3)}) m_{3/2} \quad (38)$$

In the perturbative heterotic string we expect $M \simeq M_{Pl}$ and hence $M_G/M \simeq O(10^{-2})$. If one assumes $c^{(2)}$ is real and $c^{(3)}$ is complex with arbitrary size phase, then μ naturally has a phase of size $\theta_{0\mu} \simeq O(10^{-2})$. A similar analysis can be done for the other parameters (A, B, \tilde{m}) yielding automatically small phases. One assumes only that the leading (renormalizable) term in the matter expansion is real, while the higher terms (presumably arising from integrating out the tower of massive states) can have arbitrary phases.

Other string scenarios can have $M \simeq O(M_G)$. In that case one expects the nonrenormalizable terms to give rise to large phases, unless the low lying members of the tower of heavy states do not couple to the fields of the physical sector.

V. CONCLUSIONS

In SUGRA GUT models, the basic parameters are given at the GUT scale. The renormalization group equations then carry this information to the electroweak scale, allowing for experimental tests of the model. Thus what represents a “natural” choice of parameters is presumably a GUT scale question.

The experimental values of the electric dipole moments put strong constraints on the low energy SUSY parameter space. However, for mSUGRA models at least, the RGE suppress the value of the A_t phase at the electroweak scale, α_t , so that any size of phase, α_{0A} , even $\pi/2$ at M_G will generally lead to acceptable EDMs. This effect is due to the nearness of the t-quark to its Landau pole.

The EDMs, however, are very sensitive to the B phase at the electroweak scale, θ_B . In the domain of light SUSY mass spectrum (i.e. $\lesssim 1$ TeV) and $\alpha_{0A} \simeq O(1)$, the EDMs allow a large θ_B (i.e. $O(10^{-1})$) only for low $\tan\beta$, i.e. $\tan\beta \lesssim 3$. Further, for fixed SUSY parameters in this domain, the allowed range $\Delta\theta_B$ of θ_B needed to satisfy the EDM constraints is very small for $\tan\beta \gtrsim 3$.

The above results strongly affect the GUT theory. Thus for α_{0A} large and a light mass spectrum one finds at the GUT scale that θ_{0B} is generally large, i.e. $O(1)$ even for low $\tan\beta$, and the allowed range $\Delta\theta_{0B}$ for satisfying the EDMs is exceedingly small for $\tan\beta \gtrsim 3$. Thus for this situation, θ_{0B} must be chosen large and be very precisely determined as $\tan\beta$ gets large, leading to a new fine tuning problem at the GUT scale. The origin of this difficulty resides in the requirement that the GUT models give rise to parameters at the electroweak scale that simultaneously satisfy the experimental EDM constraints and give rise to radiative electroweak breaking.

The above discussion suggests that reasonable mSUGRA models with large phases and mass spectrum below 1 TeV can only be constructed for small $\tan\beta$ i.e. $\tan\beta \lesssim 3$. The

current LEP data combined with cosmological constraints already require $\tan\beta \gtrsim 2$ [40], and LEP, the Tevatron and the LHC will be able to explore the domain $\tan\beta \lesssim 50$ [41]. Thus the value of $\tan\beta$ (or a lower bound) is something that will be determined experimentally in the not too distant future. Should $\tan\beta$ turn out to be large, it is possible that only models with small GUT phases $\phi_{0i} \simeq O(10^{-2})$ are reasonable, and it was shown above that such models can arise naturally with $\phi_{0i} \simeq O(M_G/M_{Pl})$.

Our analysis has included the loop corrections to the radiative breaking condition. While these corrections are small, they grow with $\tan\beta$ and are competitive to the θ_B contribution to the EDMs. Thus for large $\tan\beta$ (e.g. $\tan\beta \simeq 20$) they can produce a new cancellation phenomena (with $\theta_B=0$), allowing the EDM constraints to be satisfied for a light mass spectra (e.g. $m_0 \simeq 300$ GeV, $m_{1/2} \simeq 200$ GeV) which for lower $\tan\beta$ would be excluded by the EDM data.

The combined restrictions of the experimental EDM bounds for the neutron and electron put strong constraints on the SUSY parameter space. However, since the theoretical cancellations needed to satisfy experiment are delicate, as one varies the parameters one can get rather different excluded regions. Thus, while we have found that increasing m_0 gives an allowed region of smaller $m_{1/2}$ (as one might have expected), increasing $|A_0|$ can require $m_{1/2}$ to be increased to satisfy the EDM bounds. However, it should be stressed that there are significant theoretical uncertainties in the calculation of d_n , and we have seen, for example, that the current uncertainty in the quark masses m_u and m_d (arising from the uncertainty in m_s) can lead to a significant variation in the domain the neutron EDM data can exclude.

Much of the above discussion holds also for non minimal models with non universal gaugino and sfermion soft breaking masses. A more detailed discussion of the effects of non universalities will be given elsewhere [38].

VI. ACKNOWLEDGEMENT

This work was supported in part by National Science Foundation Grant No. PHY-9722090. One of us (R.A.) is pleased to acknowledge the hospitality of the Korea Institute for Advanced Study where part of this paper was written. We would also like to thank Toby Falk and Keith Olive for valuable discussions.

REFERENCES

- [1] J. Ellis, S. Ferrara and D.V. Nanopoulos, Phys. Lett. **B114**, 231 (1982); W. Buchmuller and D. Wyler, Phys. Lett. **B121**, 321 (1983); J. Polchinski and M.B. Wise, Phys. Lett. **B125**, 393 (1983).
- [2] E. Commins et al, Phys. Rev. **A 50** 2960 (1994); K. Abdullah et al, Phys. Rev. Lett. **65**, 2340 (1990).
- [3] P. G. Harris et al, Phys. Rev. Lett. **82**, 904 (1999).
- [4] J.-M. Gerard et al, Nucl. Phys. **B253**, 93 (1985); E. Franco and M. Mangano, Phys. Lett. **B135**, 445 (1984); A. Sanda, Phys. Rev. **D32**, 2992 (1985); M. Dugan, B. Grinstein and L. Hall, Nucl. Phys. **B255**, 413 (1985); W. Bernreuther and M. Suzuki, Rev. Mod. Phys. **63**, 313 (1991).
- [5] P. Nath, Phys. Rev. Lett. **66**, 2565 (1991); Y. Kizhukuri and N. Oshimo, Phys. Rev. **D45**, 1806 (1992); **D46**, 3025 (1992); R. Garisto and J. Wells, Phys. Rev. **D55**, 611 (1997).
- [6] T. Ibrahim and P. Nath, Phys. Lett. **B418**, 98 (1998).
- [7] T. Ibrahim and P. Nath, Phys. Rev. **D57**, 478 (1998).
- [8] T. Ibrahim and P. Nath, Phys. Rev. **D58**, 111301 (1998).
- [9] T. Falk and K. Olive, Phys. Lett. **B439**, 71 (1998).
- [10] S. Barr and S. Khalil, hep-ph/9903425.
- [11] T. Falk, K. Olive, M. Pospelov and R. Roiban, hep-ph/9904393.
- [12] M. Brhlik, G. Good, and G. Kane, Phys. Rev. **D 59**, 115004 (1999).
- [13] M. Brhlik, L. Everett, G. Kane and J. Lykken, hep-ph/9905215.
- [14] A. Bartl, T. Gajdosik, W. Porod, P. Stockinger and H. Stremnitzer, hep-ph/9903402.
- [15] S. Pokorski, J. Rosiek and C. A. Savoy, hep-ph/9906206.
- [16] D. Demir, hep-ph/9901389.
- [17] A. Pilaftsis and C. Wagner, hep-ph/9902371.
- [18] T. Falk, A. Ferstl and K. Olive, Phys. Rev. **D59**, 055009 (1999).
- [19] T. Falk, K. Olive and M. Srednicki, Phys. Lett. **B375**, 196 (1996).
- [20] U. Chattopadhyay, T. Ibrahim and P. Nath, hep-ph/9811362.
- [21] A. Pilaftsis, hep-ph/9803297; hep-ph/9805373.
- [22] A. Chamseddine, R. Arnowitt and P. Nath, Phys. Rev. Lett. **49** 970 (1982); for reviews see P. Nath, R. Arnowitt and A. Chamseddine, *Applied N=1 Supergravity*, World Scientific (1984); H. P. Nilles, Phys. Rep. **110**,1 (1984).
- [23] E. Cremmer, S Ferrara, L. Girardello and A. Van Proeyen, Phys. Lett. **B116**, 231 (1982); Nucl. Phys. **B212**, 413 (1983).
- [24] E. Witten and J. Bagger, Nucl. Phys. **B222**, 125 (1983).
- [25] D. Chang, W-Y. Keung and A. Pilaftsis, Phys. Rev. Lett. **82**, 900 (1999).
- [26] Dai et al, Phys. Lett. **B237**, 216 (1990).
- [27] R. Arnowitt, J. L. Lopez, D.V. Nanopoulos, Phys. Rev. **D42**, 2423 (1990); R. Arnowitt, M. Duff and K. Stelle, Phys. Rev. **D43**, 3085 (1991).
- [28] A. Manohar and H. Georgi, Nucl. Phys. **B234**, 189 (1984).
- [29] H. Leutwyler, Phys. Lett. **B374**, 163 (1996).
- [30] R. Gupta and T. Bhattacharya, Phys. Rev. **D55**, 7203 (1997); B. Gough et al Phys. Rev. Lett. **79**, 1622 (1997).
- [31] R. Burkhalter, hep-lat/9810043,

- [32] L.E. Ibanez and C. Lopez, Nucl. Phys. **B233**, 511 (1984); L.E. Ibanez, C. Lopez and C. Munoz, Nucl. Phys. **B256**, 218 (1985).
- [33] M.S. Alam et.al (CLEO collab.), Phys. Rev. Lett. **74**, 2885 (1995).
- [34] S. Bertolini, F. Borzumati, A. Masiero and G. Ridolfi, Nucl. Phys. **B353**, 591 (1991); J. Wu, R. Arnowitt and P. Nath, Phys. Rev. **D51**, 1371 (1995); V. Barger, M. Berger, P. Ohmann and R. Phillips, Phys. Rev. **D51**, 2438 (1995).
- [35] V. Barger, M. Berger and P. Ohmann, Phys. Rev. **D49**, 4908 (1994).
- [36] P. Nath, J. Wu and R. Arnowitt, Phys. Rev. **D52**, 4169 (1995).
- [37] G. Gamberini, G. Ridolfi and F. Zwirner, Nucl. Phys. **B331**, 331 (1990); R. Arnowitt and Pran Nath, Phys. Rev. **D46**, 3981 (1992).
- [38] E. Accomando, R. Arnowitt and B. Dutta, work in progress.
- [39] A. Masiero and H. Murayama; hep-ph/9903363; K.S. Babu, B. Dutta and R.N. Mohapatra, hep-ph/9905464; S. Khalil and T. Kobayashi, hep-ph/9906374.
- [40] J. Ellis, T. Falk, K. Olive and M. Srednicki, hep-ph/9905481.
- [41] M. Carena, S. Mrenna and C. Wagner, hep-ph/9907422.

FIGURES

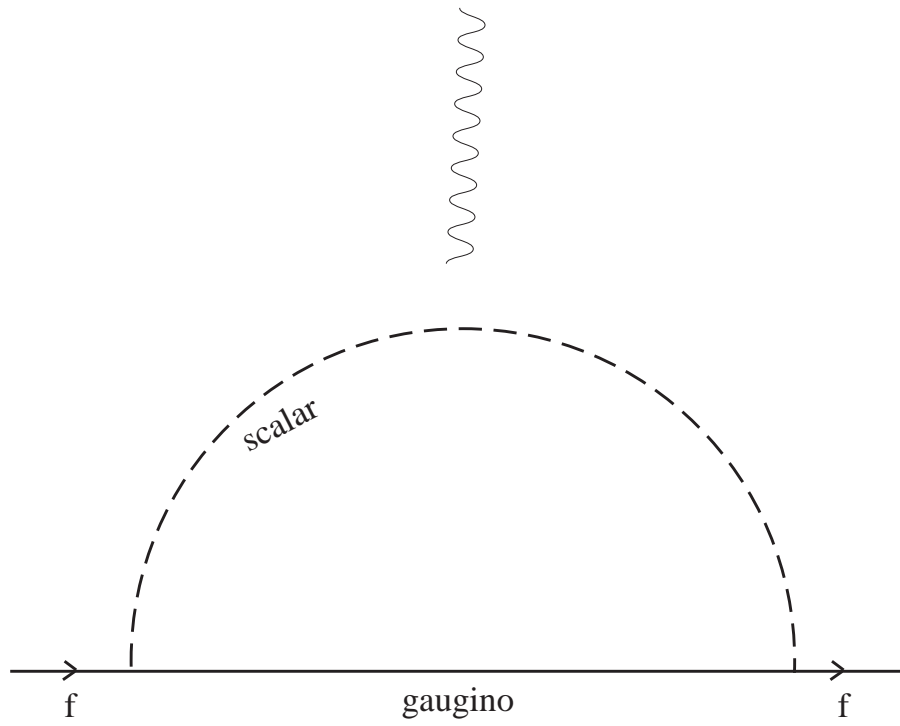


FIG. 1. One loop diagram. The photon line can be attached to any charged particle.

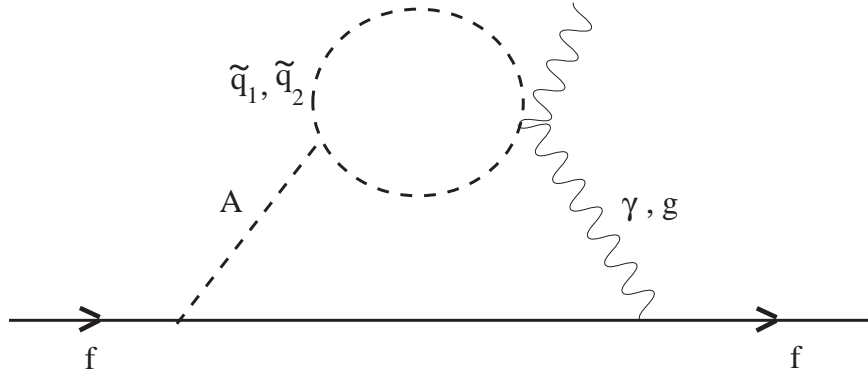
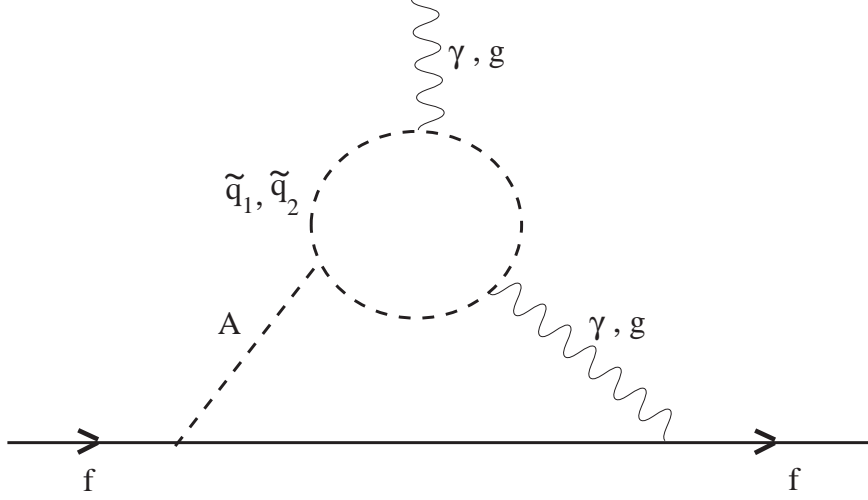


FIG. 2. Two loop Barr-Zee diagrams. A is the CP odd Higgs and \tilde{q}_i are the mass diagonal squark states.

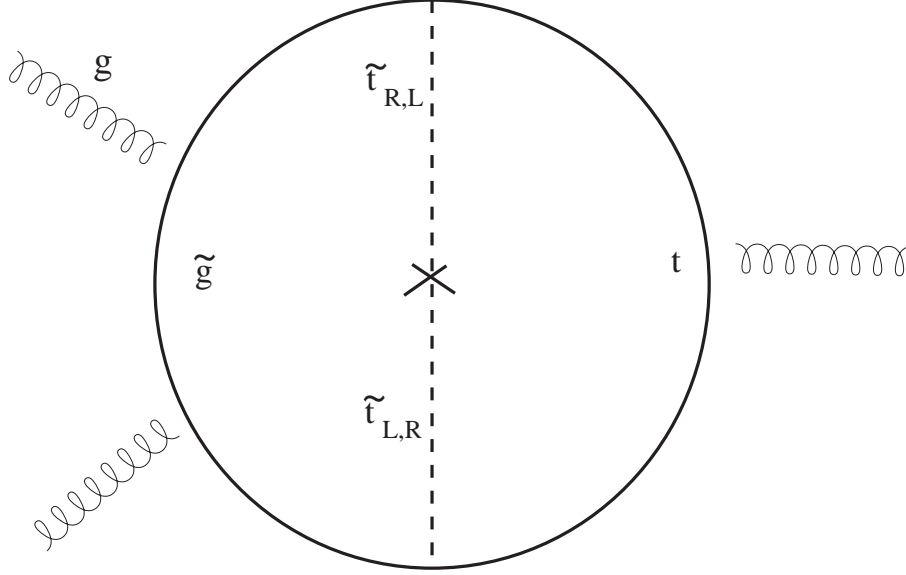


FIG. 3. Two loop Weinberg type diagram.

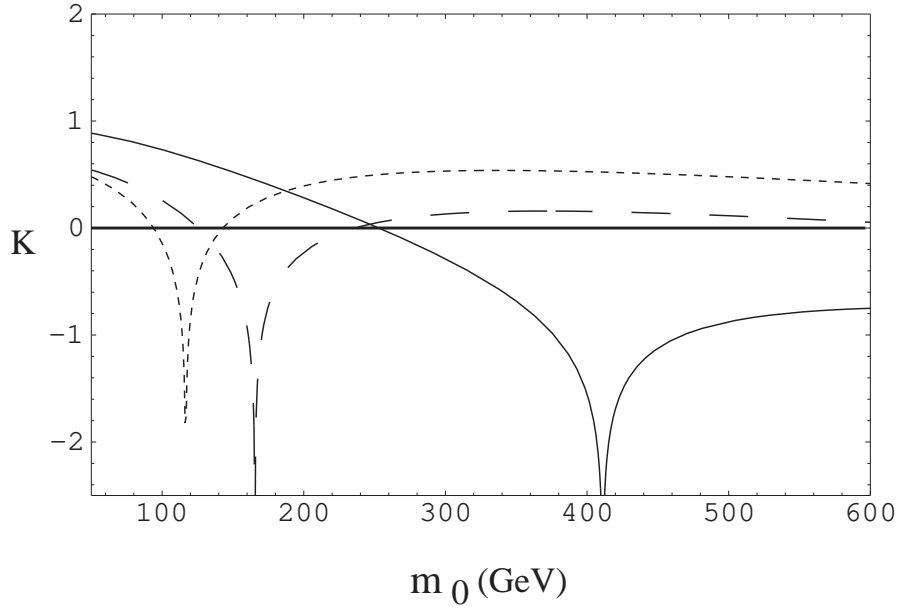


FIG. 4. K (defined in the text) is plotted as a function of m_0 for d_e . The solid, dashed and dotted lines are for $\tan\beta = 3, 10$ and 20 respectively. The other input parameters are $\alpha_{0A} = \frac{\pi}{2}$, $|A_0| = 300$ GeV, $\theta_B = 0.02$ and $m_{1/2} = 300$ GeV.

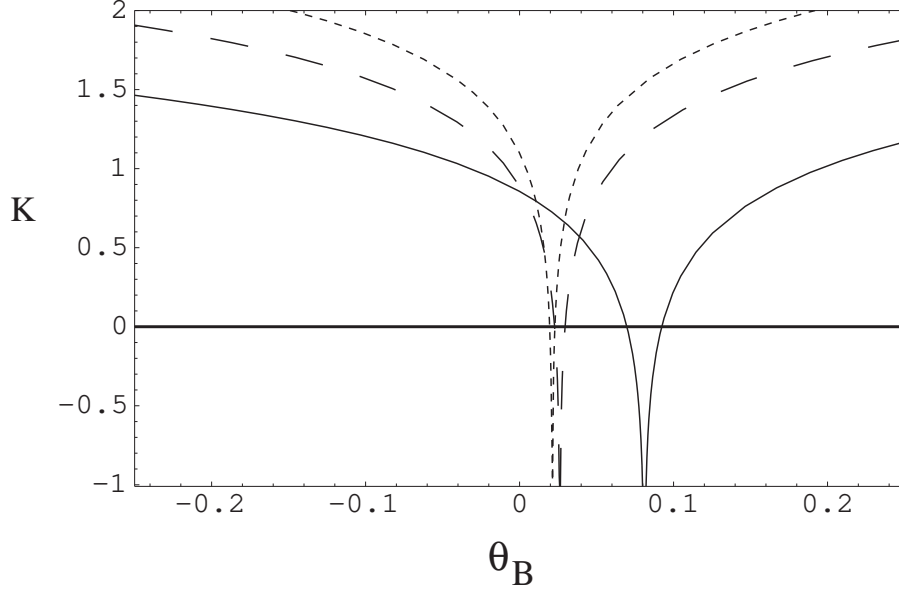
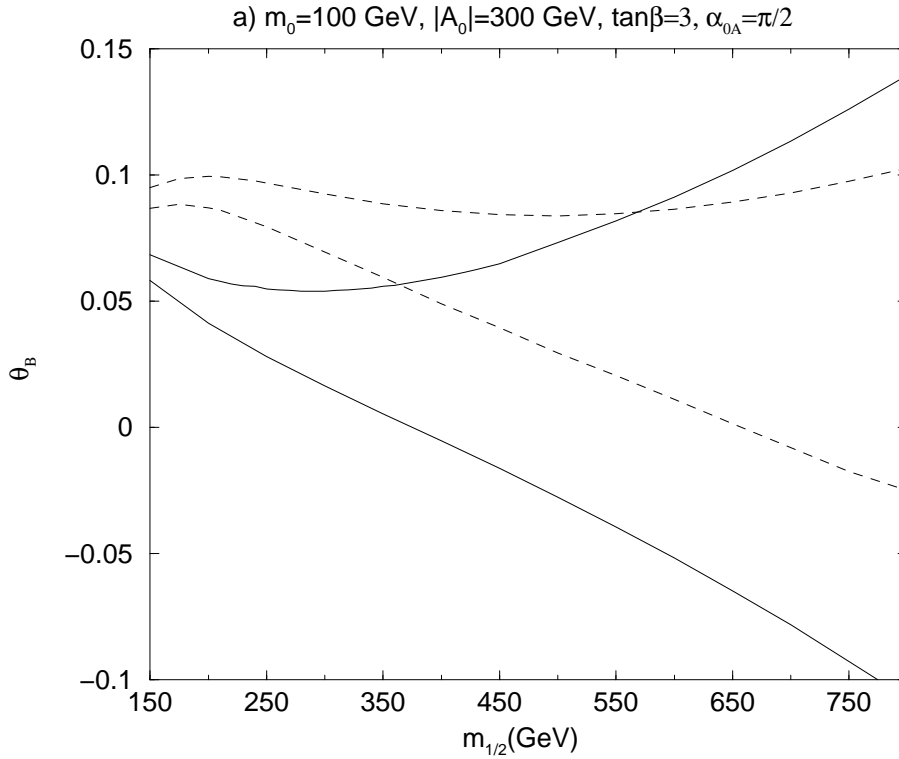


FIG. 5. K (for eEDM) is plotted as a function of θ_B . The solid, dashed and dotted lines are for $\tan\beta = 3, 10$ and 20 respectively. The other input parameters are $\alpha_{0A} = \frac{\pi}{2}$, $|A_0| = 300$ GeV, $m_{1/2} = 300$ GeV and $m_0 = 100$ GeV.



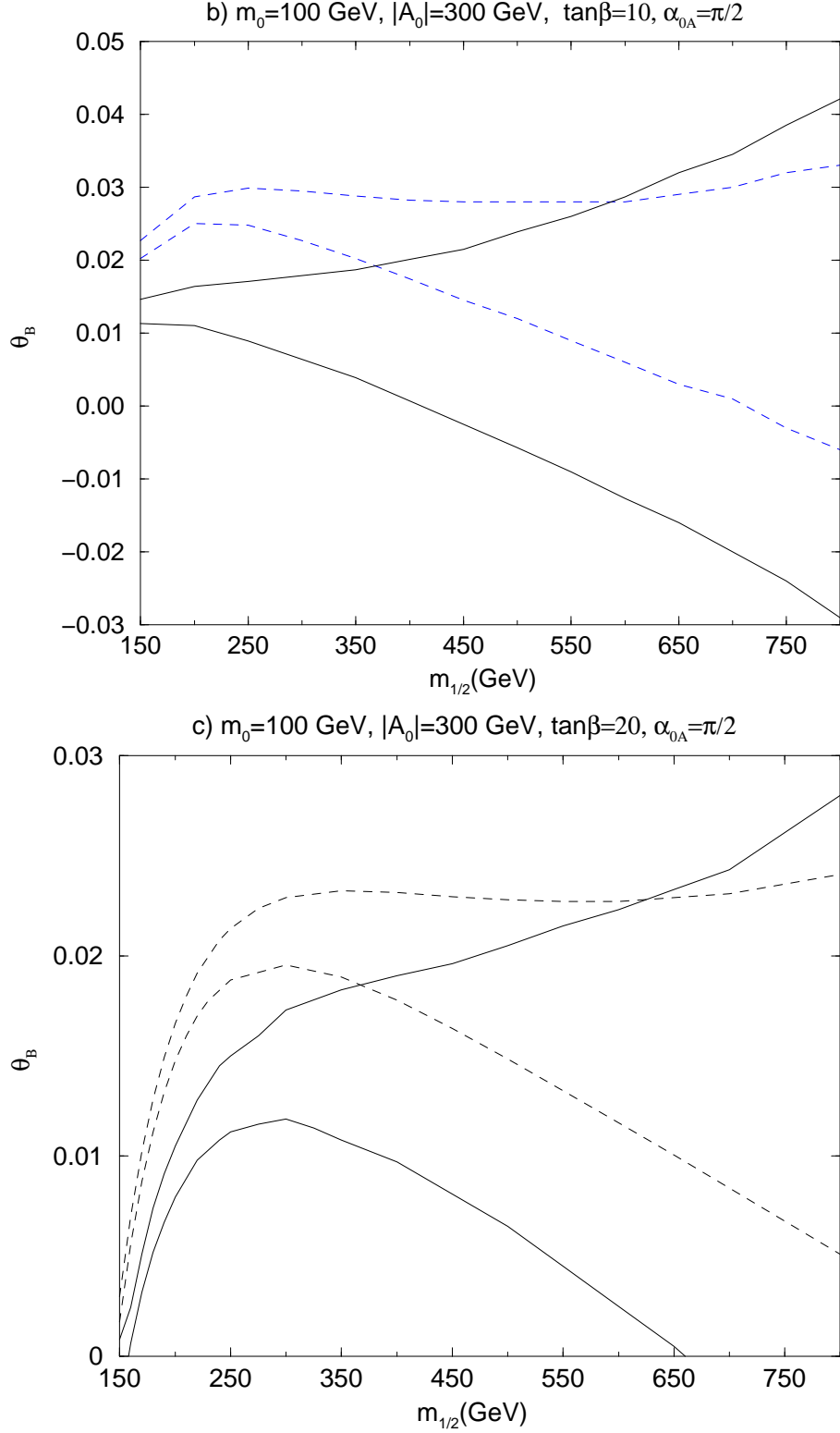
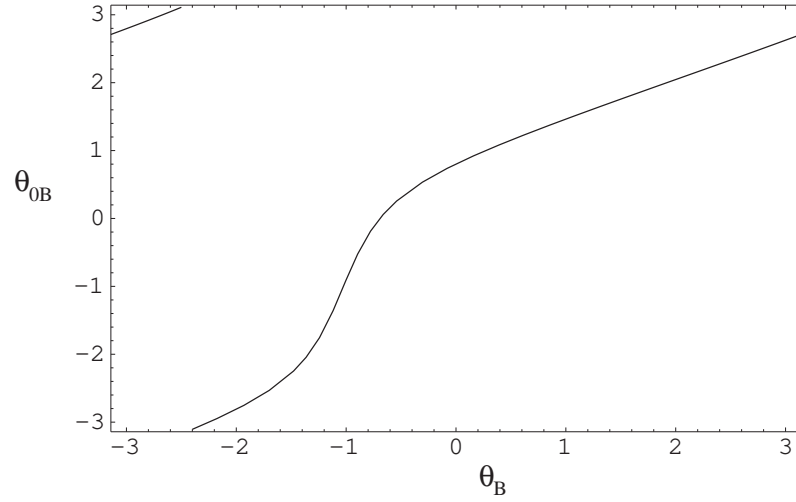
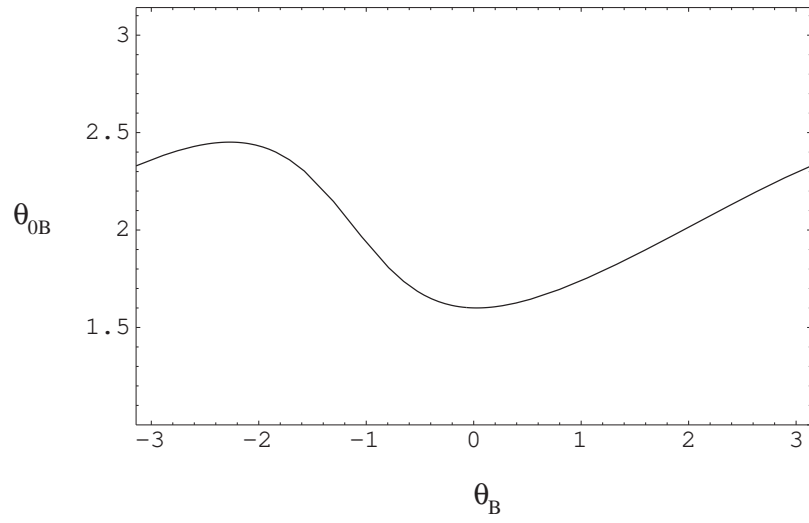


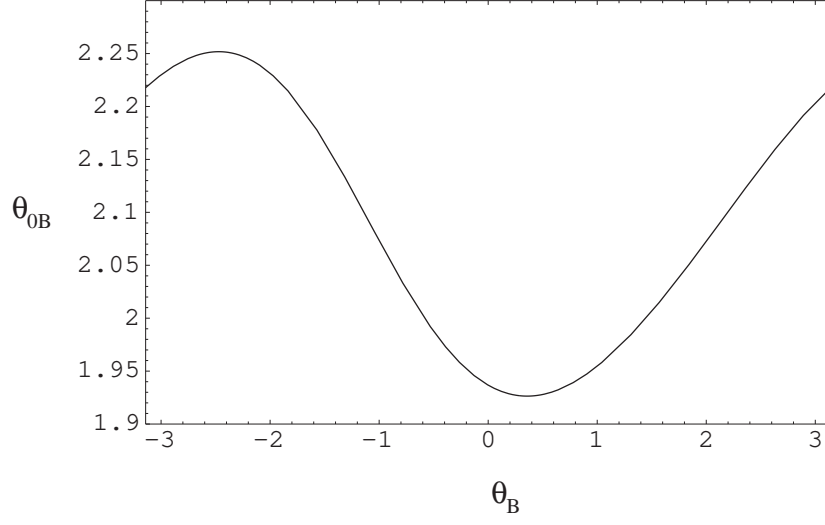
FIG. 6. The $K=0$ contours plotted as a function of θ_B and $m_{1/2}$. The solid lines are for d_n and the dotted lines are for d_e .



a)

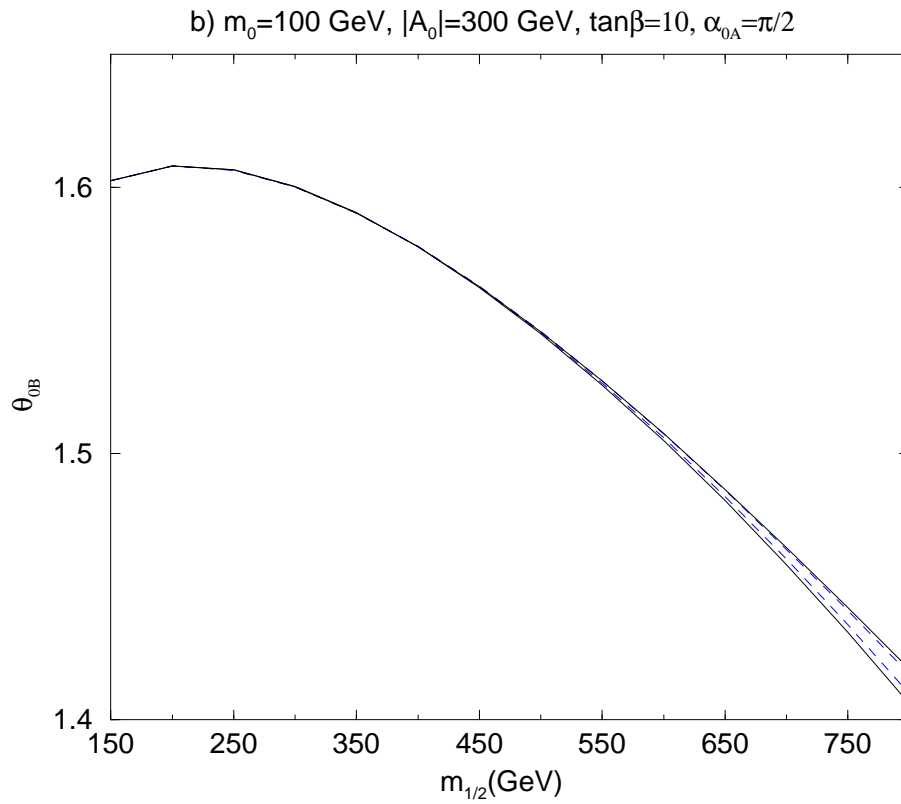
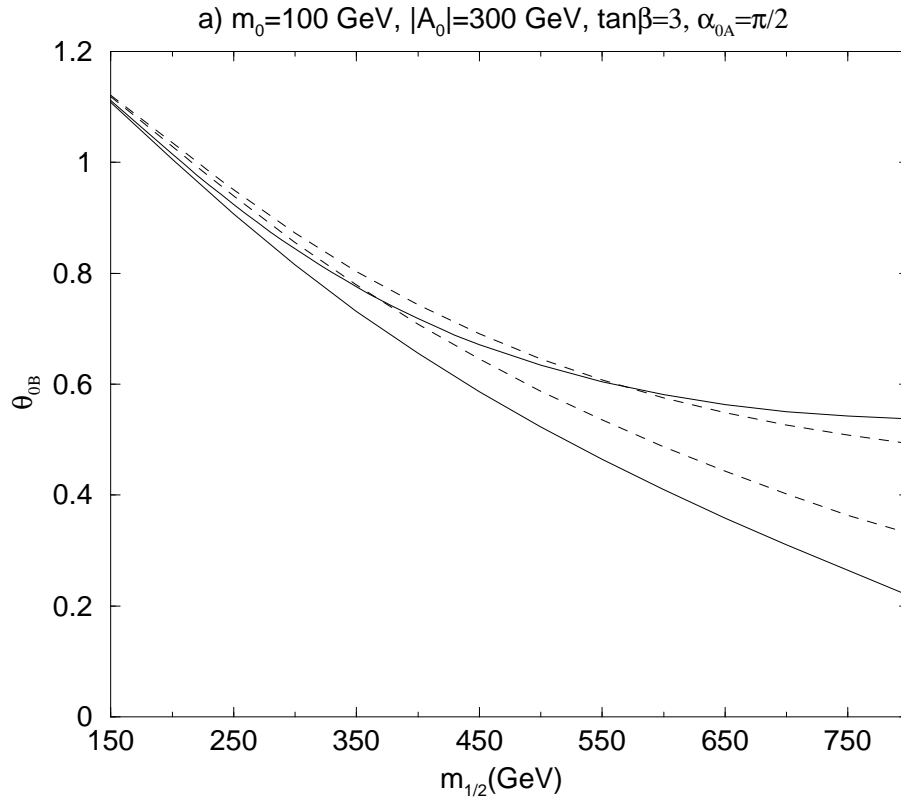


b)



c)

FIG. 7. θ_{0B} is plotted as a function of θ_B . Figs. a, b and c are for $\tan\beta = 3, 10$ and 20 respectively. The other input parameters are $\alpha_{0A} = \frac{\pi}{2}$, $|A_0| = 300$ GeV, $m_0 = 100$ GeV and $m_{1/2} = 300$ GeV.



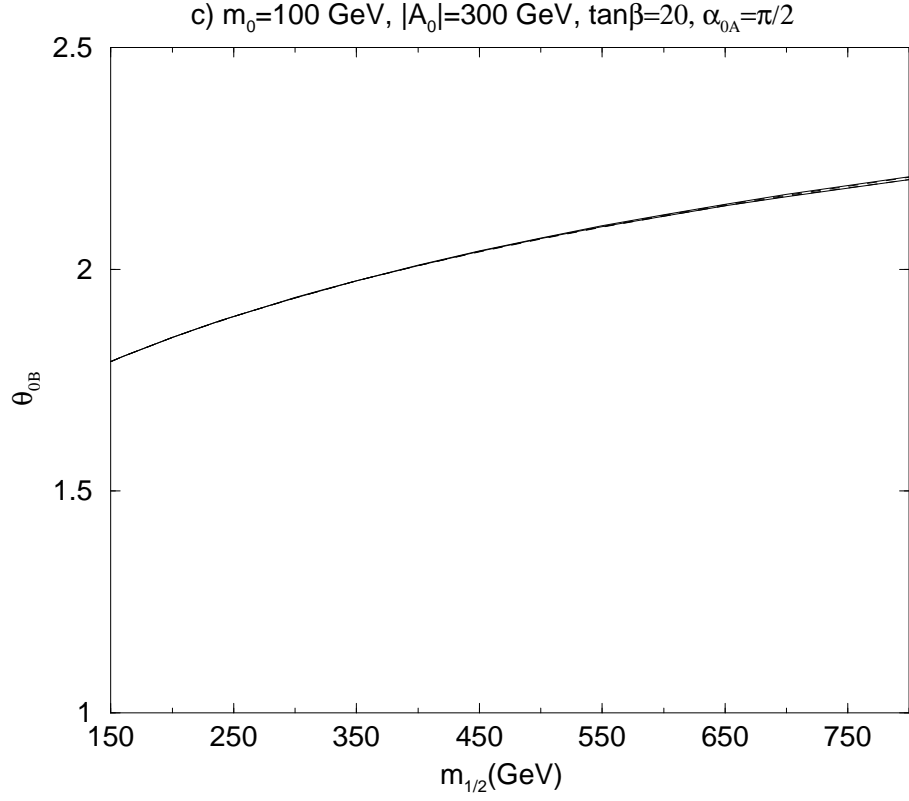


FIG. 8. θ_{0B} vs $m_{1/2}$. Upper and lower lines are the allowed range so that $K \leq 0$. The solid lines are for d_n and the dotted lines are for d_e .

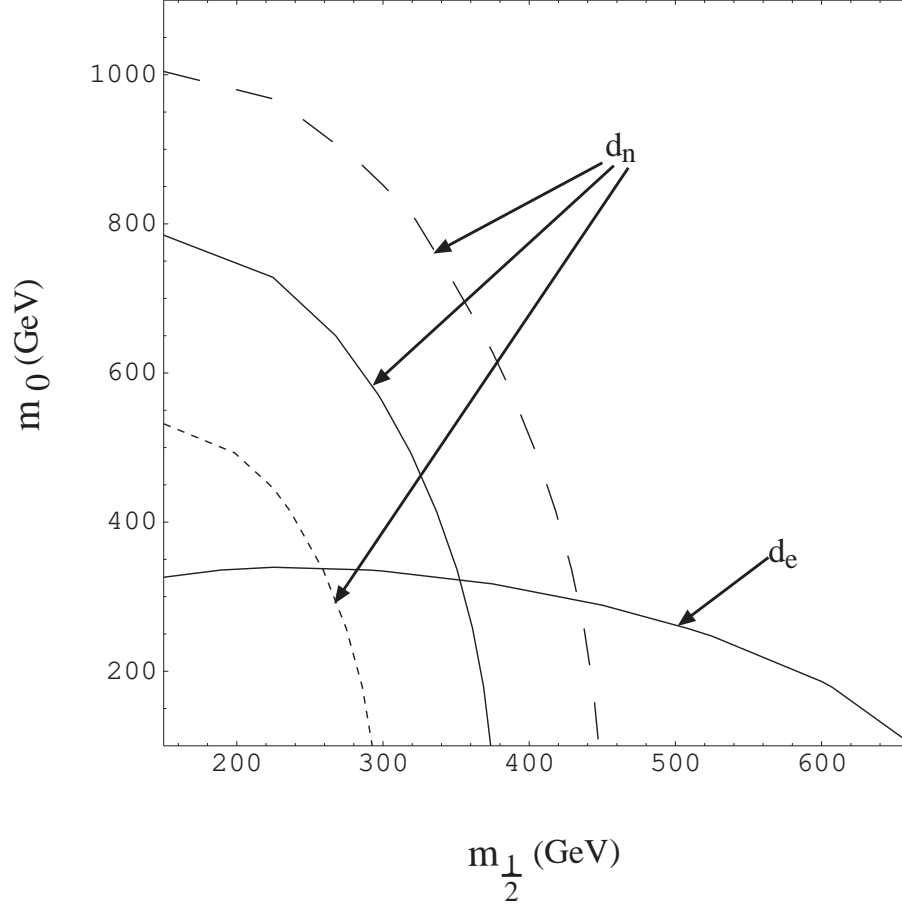


FIG. 9. The $K=0$ contours are plotted as a function of m_0 and $m_{1/2}$. The dotted, solid and dashed lines are for m_d (1 GeV)=5, 8 and 12 MeV respectively. The other input parameters are $\alpha_{0A} = \frac{\pi}{2}$, $|A_0| = 300$ GeV $\theta_B=0$ and $\tan\beta=3$. Excluded regions are below d_e and to the left of d_n curves.

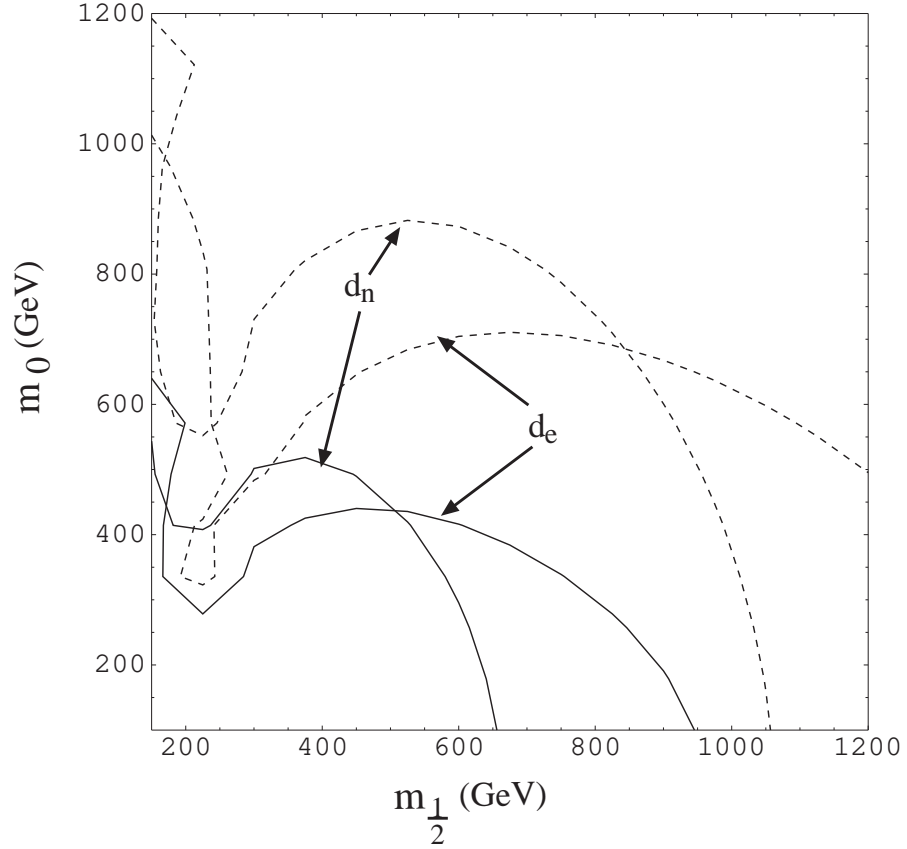


FIG. 10. Allowed region in $m_0 - m_{1/2}$ plane for d_e and d_n . The other input parameters are $\alpha_{0A} = \frac{\pi}{2}$, $|A_0| = 300$ GeV, $\theta_B=0$ and $\tan\beta=20$. The solid lines are for $K=0$ and the dotted lines are for $K=-0.5$.

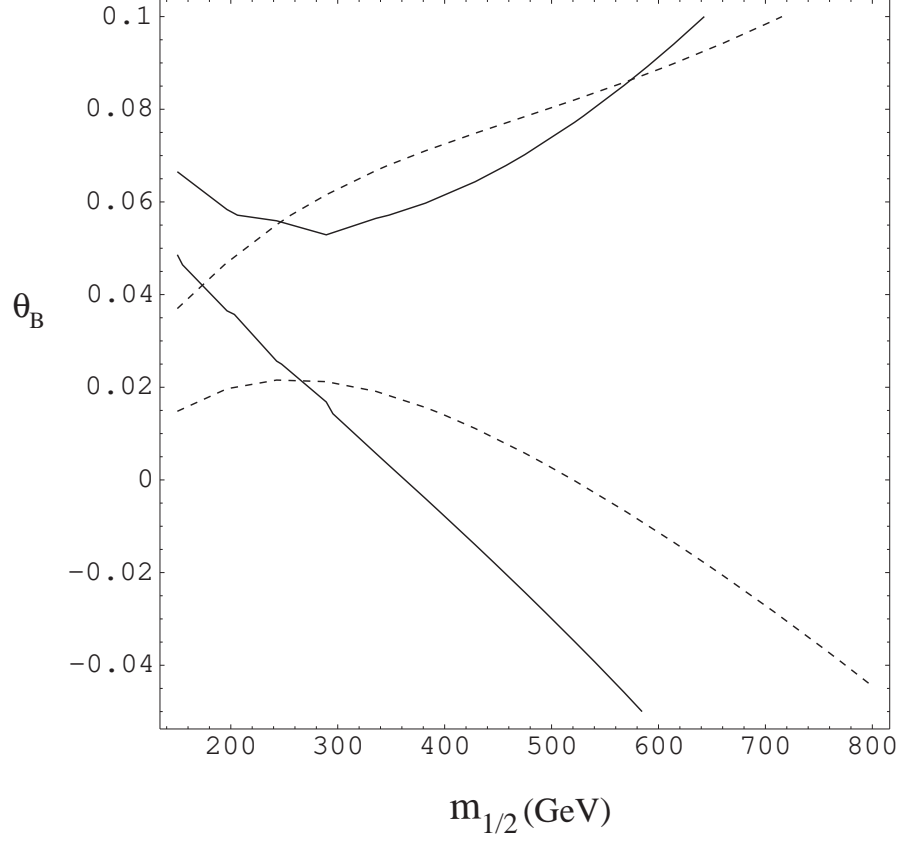


FIG. 11. The $K=0$ contours are plotted as a function of θ_B and $m_{1/2}$, where $\alpha_{0A} = \frac{\pi}{2}$, $|A_0| = 300$ GeV, $m_0=250$ GeV and $\tan\beta=3$. The solid lines are for d_n and the dotted lines are for d_e .

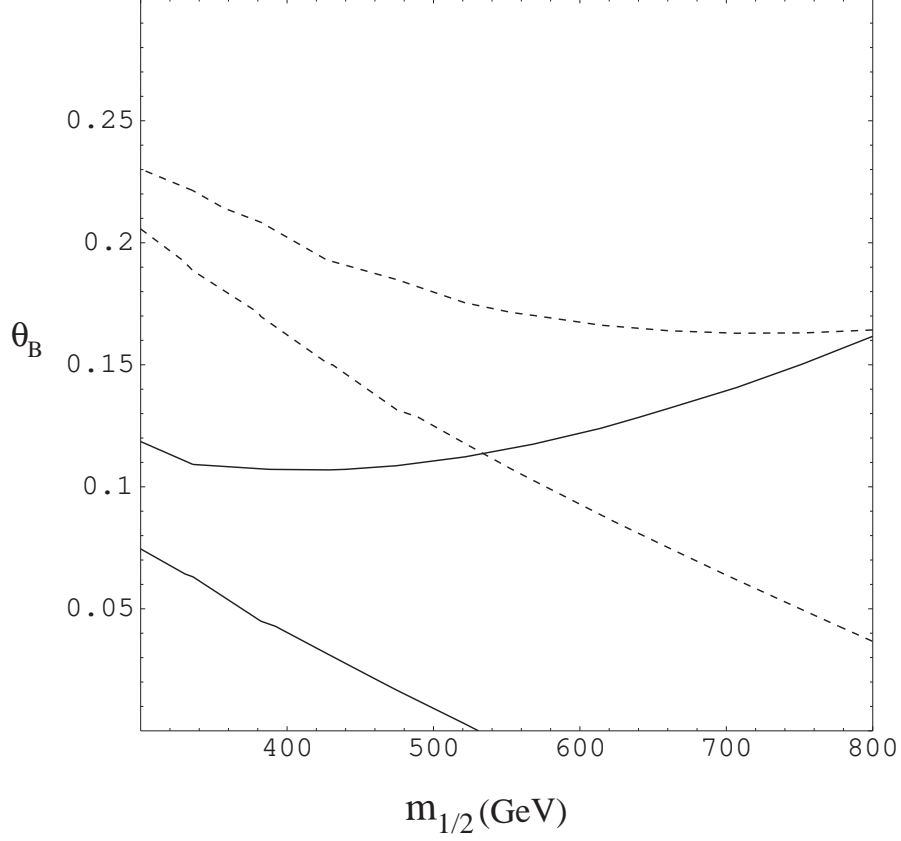


FIG. 12. The $K=0$ contours are plotted as a function of θ_B and $m_{1/2}$, where $\alpha_{0A} = \frac{\pi}{2}$, $|A_0| = 800$ GeV, $m_0=100$ GeV and $\tan\beta=3$. The solid lines are for d_n and the dotted lines are for d_e .

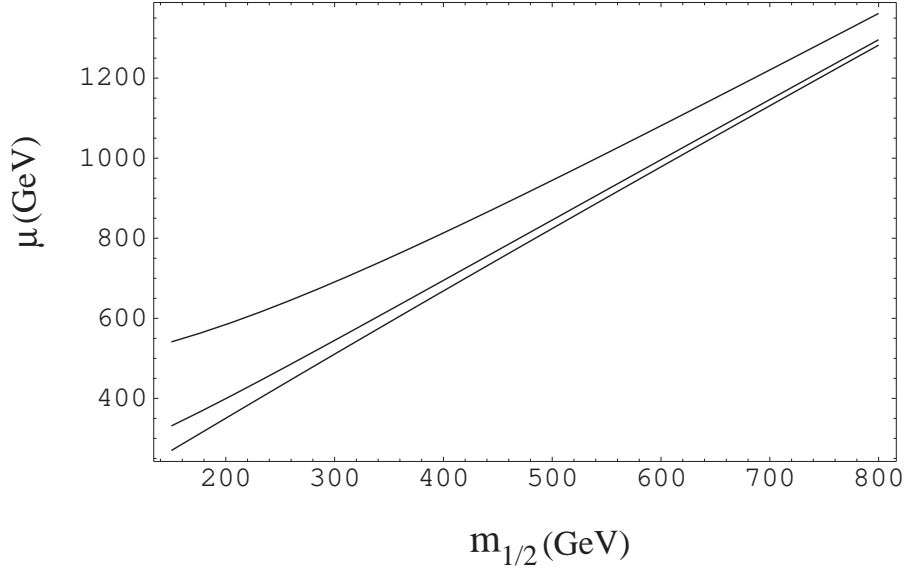


FIG. 13. The parameter $|\mu|$ is plotted as a function of $m_{1/2}$. The three solid lines are for $m_0 = 700$ (top), 300 (middle) and 100 (bottom) GeV. The other input parameters are $\alpha_{0A} = \frac{\pi}{2}$, $|A_0| = 300$ GeV, $\tan\beta=3$ and $\theta_B = 0.08$.

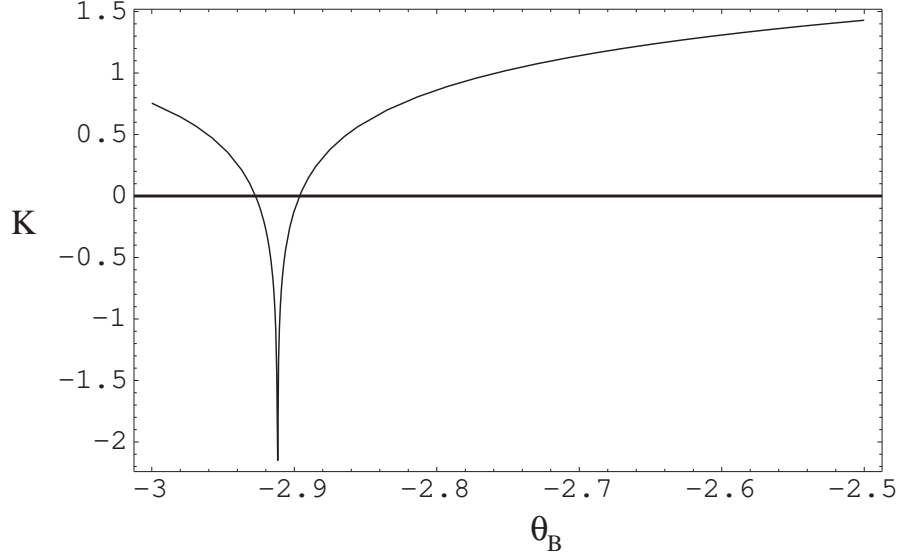


FIG. 14. K (for d_e) as a function of θ_B . The other input parameters are $m_0=200$ GeV; $m_{1/2i}=150$ GeV, $\tan\beta=3$, $\alpha_{0A} = \frac{\pi}{2}$, $|A_0| = 100$ GeV and $\phi_1 = 4\pi/5 = \phi_3$.

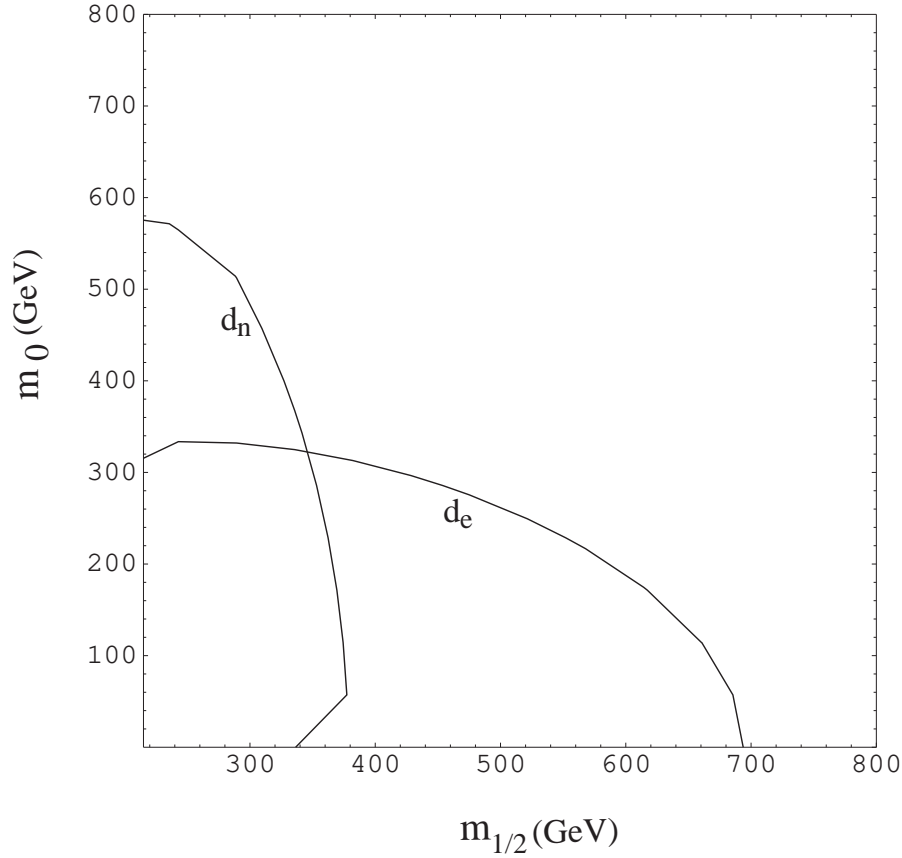


FIG. 15. Allowed region in $m_0 - m_{1/2}$ plane ($K \leq 0$) in a nonuniversal scenario. The other input parameters are $\alpha_{0A} = \frac{\pi}{2}$, $\theta_B = 0$, $|A_0| = 300$ GeV, $\tan\beta=5$, $\delta_1=1$, $\delta_2=-1$, $\delta_{10}=-1$ and $\delta_5=-0.3$.